Uniaxial strain induced band splitting in semiconducting SrTiO_{3}

Young Jun Chang, Guru Khalsa, Luca Moreschini, Andrew L. Walter, Aaron Bostwick, Karsten Horn, A. H. MacDonald, and Eli Rotenberg

Phys. Rev. B **87**, 115212 — Published 29 March 2013

DOI: 10.1103/PhysRevB.87.115212

Uniaxial strain induced band splitting in semiconducting $SrTiO_3$

Young Jun Chang,[1,2,3,*] Guru Khalsa,[4] Luca Moreschini,[1] Andrew L. Walter,[1,2]
Aaron Bostwick,[1] Karsten Horn,[2] A. H. MacDonald,[4] Eli Rotenberg,[1]

[1] *Advanced Light Source (ALS), E. O. Lawrence Berkeley National Laboratory, Berkeley, California 94720, USA,*
[2] *Department of Molecular Physics, Fritz-Haber-Institut der Max-Planck-Gesellschaft, Faradayweg 4-6, 14195 Berlin, Germany,*
[3] *Department of Physics, University of Seoul, Seoul 130-743, Korea,*
[4] *Department of Physics, University of Texas at Austin, 1 University Station C1600, Austin, TX 78712, USA**

(Dated: February 4, 2013)

We use angle resolved photoemission spectroscopy to study the influence of mechanically induced uniaxial strain on the electronic structure of the oxide semiconductor $SrTiO_3$. We observe an orbital splitting between the Ti $3d_{yz}$ and $3d_{xy}$ bands, which are degenerate when unperturbed. Using the **k·p** method, we qualitatively explain the direction and the size of the observed energy splitting. Our comprehensive understanding of band splitting explains the strain-induced mobility enhancement of electron-doped $SrTiO3_3$ in terms of band degeneracy breaking and reduced interband scattering. Our approach can be extended to differently strained oxide systems.

PACS numbers: 71.20.-b, 71.70.Fk, 79.60.Bm

I. INTRODUCTION

Strain can play a vital role in controlling the physical properties of crystals. Changes in the band structure, such as band splitting and warping, can be triggered by small variations in the lattice parameters. Sizable strain-induced modifications of the electronic structure have been observed in various materials ranging from metals[1,2] and semiconductors,[3,4] to oxides.[5–7] Semiconductors with degeneracies at band edges, such as those that occur at the top of the valence band in silicon and germanium, are especially sensitive to strain. For this reason both uniaxial and biaxial strain engineering have been successfully applied to improve current semiconductor electronics technology while maintaining the traditional device fabrication process.[4]

The oxide semiconductor $SrTiO_3$ and its heterostructures have attracted much attention for the energy-harvesting applications, such as solar water splitting[8] and its use in thermoelectric devices,[9] the efficiency of which can be improved by tuning the band gap or electron mobilities, and for the next-generation electronic device applications,[10] in which superconductivity,[11] magnetism,[12] and interface orbital reconstruction[13] may become important. Control of these properties can be driven by our understanding of the band structure changes upon induced strain.[14–16] Recent experiments suggest that the mobility of STO can be enhanced by a factor of three under uniaxial compressive strain,[14] demonstrating the potential of strain-engineering in oxide semiconductors. Moreover, theoretical calculations on $SrTiO_3$ have shown that anisotropic strains can reduce the band gap, which is a key driver to improving efficiency of solar energy harvest, by breaking degeneracies at the band edges.[15] In spite of a considerable effort, at present a comprehensive picture of the strain-triggered electronic structure changes is missing even in this widely studied material.

$SrTiO_3$has a cubic perovskite structure with a cubic-tetragonal structural phase transition at a temperature of 105 K. Oxygen vacancies or cation dopants (Nb or La) induce electron-doping, lowering the degenerate conduction bands (three t_{2g} orbital bands (d_{xy}, d_{yz}, d_{xz})) below the Fermi level. Indeed, even the small tetragonal distortion ($\sim 0.05\%$) below 105 K lifts the degeneracy by lowering the d_{xy} states below the other two bands.[17] Therefore, above the cubic-tetragonal structural phase transition temperature, the degenerate band structure of $SrTiO_3$ should be sensitive to external stress.

Here we study the effect of mechanically induced uniaxial strain on the degenerate conduction band structure of the electron-doped $SrTiO_3$. We observe the degeneracy breaking in the strained region, where a finite energy splitting appears, compared to the degenerate band structure in the unstrained region. We interpret the observed effects in terms of a **k·p** model and estimate the strength of the associated deformation potential.

II. EXPERIMENTAL

We apply a uniaxial strain to $SrTiO_3$ single crystals ($5\times5\times0.1$ mm) in a three-point bending geometry. Figure 1(a) shows a schematic of the bent crystal, pushed up at the center with a thin piece of tantalum foil and clamped at both sides. The resulting curvature of the crystal shows two distinct regions, *i.e.*, the central curved region with tensile strain (S) and the side regions with nearly no strain (NS1,2). We estimate the amount of the tensile strain as $\sim 0.26\%$ from the lateral width ($\sim$ 1 mm) of the S region and the tilt angle (2°) between the two side regions.[14] The crystal is annealed in ultra high vacuum to introduce an electron concentration of about $10^{20}\ cm^{-3}$, as we reported previously.[17]

The strained $SrTiO_3$ crystal shows a sharp low-energy electron diffraction (LEED) pattern. Figure 1(b-d) show the (1,-1) spots taken at the three different regions with the same sample alignment. While LEED shows a sharp spot at the NS regions, in the S region it gives an elongated spot. This is due to the large electron beam diameter ($>$ 1 mm) of the LEED electron gun, which exceeds the 1 mm-long curved region. Therefore, the line profile along the horizontal axis indicates that the elongated spot consists of a combination of the sharp

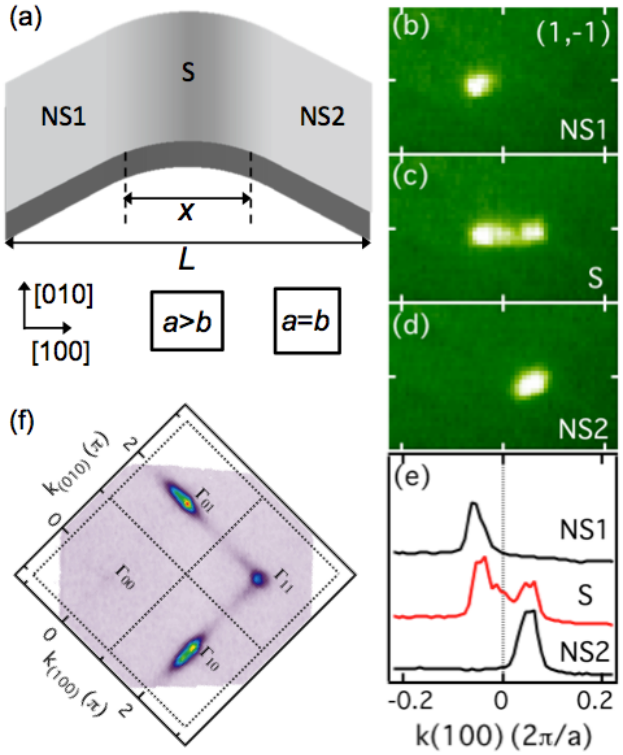

FIG. 1. (color online) (a) A thin $SrTiO_3$ (001) single crystal is bent at the center (S) where the crystal is maximally curved, while both sides remain without a significant curvature (non-strained: NS). a and b represent the in-plane lattice constants. (b)-(d) (1,-1) LEED spot images taken at different locations in the same sample. The curved crystal surface changes the spot position and elongated the spot at the center where the LEED electron beam is larger than the S region. (e) Line profiles of the (1,-1) LEED spots in b-d along the horizontal axis. (f) Fermi surface cut of the electron-doped $SrTiO_3$ when rotated by 45° relative to the electron spectrometer's horizontal entrance slit. ($SrTiO_3$ lattice constant a = 3.905 Å and π/a = 0.805 $Å^{-1}$)

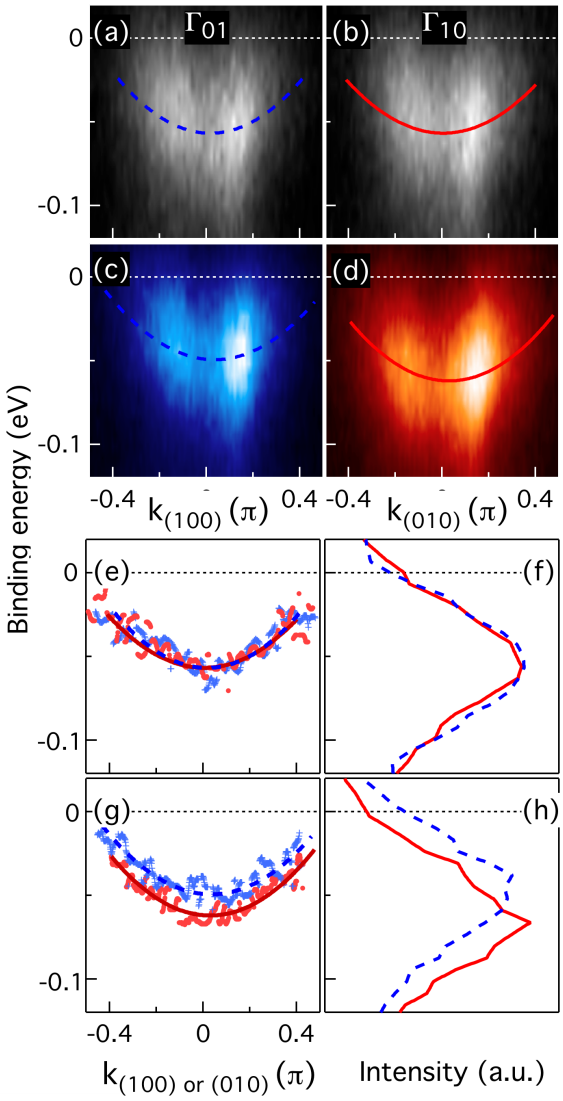

FIG. 2. (color online) The energy-distribution curves of $SrTiO_3$ for ((a)-(d)) strained and [(e)-(h)] non-strained region near the Fermi level. The band structure cuts are taken for ((a) and (e)) BZ [01] and ((b) and (f)) BZ [10] along k(100) and k(010) axes in Fig. 1(b), respectively. (c,g) Dispersions of peak positions in the energy-distribution curves with parabolic fitting lines. (d,h) Energy-distribution curves taken at k(100)(or k(010)) = 0.

spots taken in the side regions, as shown in Fig. 1(e).

The ARPES measurements were performed at the Electronic Structure Factory endstation at beamline 7.0.1 of the Advanced Light Source, equipped with a hemispherical Scienta R4000 electron analyzer. We conducted measurements at a sample temperature at 130 K using a photon energy of $\sim$ 100 eV and an overall energy resolution of 25 meV. The small spot size of the photon beam (50 μm) prevents any overlapping of the signal from the S and NS regions.

III. RESULTS AND ANALYSIS

Figure 1(f) shows the Fermi surface cut of electron-doped $SrTiO_3$ measured over a wide momentum range. Since the light polarization is even with respect to the scattering plane, our measurement geometry allows us to access only the even initial states. The ensuing matrix element effects are very strong in $SrTiO_3$ (001), and have been explained in detail elsewhere.[18] Electron-doped bulk $SrTiO_3$ has three degenerate conduction bands, i.e. Ti d_{xy}, d_{yz}, and d_{xz}states, corresponding to three perpendicular ellipsoidal Fermi surfaces.[17] The three degenerate Ti $3d$ t_{2g} states exchange their spectral weight among different Brillouin zones (BZs). For example, whereas no bands are visible in the [00] BZ, all are present in the [11] BZ, while the d_{yz} and d_{xz} bands are measured separately in the BZ [01] and [10], respectively. Since they do not show overlapping features from different states, the [01] and [10] BZs are the preferable choice for our measurement in order to get the clearest photoemission images of the respective

electronic states.

Figure 2 compares the band dispersion in the S and NS regions. The ARPES maps are taken near the Γ_{01} and Γ_{10} points along k(100) or k(010) directions, *i.e.*, along the major axis of the ellipsoidal constant energy contour. In the NS regions, the d_{yz} (Fig. 2(a)) and d_{xz} (Fig. 2(b)) states disperse with the characteristic electron-like parabola with minimum at a binding energy of $\sim$ 55 meV. On the other hand, in the S region (Fig. 2(c,d)), we observe clear changes of binding energies of the two orbital bands shifting in opposite directions.

This is shown more quantitatively in the energy distribution curve (EDC) analysis. The peak position of the EDCs, shown in symbols in Fig. 2(e,g), are fitted by parabolic functions, shown as dashed and solid curves in Fig. 2(a-e,g). The dispersion curves in Fig. 2(e) can be perfectly superimposed since the d_{xz} and d_{yz} states are degenerate, reproducing our previous result in unstrained $SrTiO_3$.[17] Conversely, in Fig. 2(g), the d_{yz} dispersion is lifted by 8 meV while the d_{xz} state is lowered by 5 meV. The difference becomes even more evident in the comparison of EDCs at Γ points, as shown in Fig. 2(h). As a whole, the strained region shows a band splitting of about 13 meV.

We have carefully tried to identified the changes caused by the external strain alone. The sample temperature was chosen to be at 130 K so that the $SrTiO_3$ single crystal remains cubic unless the external strain is applied. The effect of two possible systematic errors[19] has been minimized by orienting the crystal as shown in Fig. 1(f) relative to the electron spectrometer. We precisely choose the band structure cuts along each Γ-X direction of the two BZs from wide momentum space scans. Finally, we compared the measurements taken in the two different regions (S and NS) in one and the same to rule out the influence of local variations in sample quality. All these aspects minimize the systematic errors and ensure that the energy shifts in the S region is a genuine effect of uniaxial strain.

For a deeper understanding, we apply the **k**·**p** theory to model changes of the conduction band structure in $SrTiO_3$. This method is widely used to describe the band edges of strained semiconductors.[3] Its application to d^0 perovskites has been described by Bistritzer et al.[18] Here we focus on the changes to the conduction band structure in $SrTiO_3$ due to an externally applied strain and assume that the spin-orbit splitting is below the experimental resolution.

Application of an external strain deforms the ionic potential and thus changes the crystal symmetry of the unit cell. Including this influence in the **k**·**p** theory results in a perturbation Hamiltonian of the form:

$$H' = \sum_{i,j} \left(-\frac{p_i p_j}{m_0} + \delta V_{ij} \right) \epsilon_{ij} \tag{1}$$

where p_i, m_0, δV_{ij}, and ϵ_{ij} are the ith component of the momentum, bare electron mass, change in the ionic potential, and components of the strain tensor, respectively.[3,20] Here we have assumed inversion symmetry in the unstrained crystal structure. This perturbation Hamiltonian is then evaluated for the t_{2g} bands. The strain-induced change in the Hamiltonian has the form,

$$H'_{t_{2g}} = \begin{pmatrix} l\epsilon_{11} + m\left(\epsilon_{22}+\epsilon_{33}\right) & n\epsilon_{12} & n\epsilon_{13} \\ n\epsilon_{21} & l\epsilon_{22} + m\left(\epsilon_{33}+\epsilon_{11}\right) & n\epsilon_{23} \\ n\epsilon_{31} & n\epsilon_{32} & l\epsilon_{33} + m\left(\epsilon_{11}+\epsilon_{22}\right) \end{pmatrix} \tag{2}$$

written in the $\{ d_{yz}, d_{xz}, d_{xy} \}$ basis. Here l, m, and n are the deformation potentials which can be extracted from our experimental data. For a uniaxial tensile strain along the x-axis, $\epsilon_{11} = \epsilon$ and $\epsilon_{22} = \epsilon_{33} = -\nu\epsilon$ where ν is the Poisson ratio. All other strain components are zero. The perturbation Hamiltonian then simplifies to,

$$\begin{pmatrix} (l-2m\nu)\epsilon & 0 & 0 \\ 0 & (m(1-\nu)-l\nu)\epsilon & 0 \\ 0 & 0 & (m(1-\nu)-l\nu)\epsilon \end{pmatrix} \tag{3}$$

We find a Γ point splitting of $(l-m)(1+\nu)\epsilon$ between the d_{yz} band and the remaining t_{2g} bands. Because the relative change in the lattice constant along the x-axis is known from the geometry, comparing the splitting at the Γ point gives a direct measure of the deformation potentials relevant to the uniaxial strain ($\epsilon = 0.0026$). We find $l-m \approx 4.03$ eV, where we have used the Poisson ratio at 130K, $\nu = 0.242$ calculated from the stiffness constants reported in Refs. 21 and 22. We also note that the estimated deformation potential is similar in scale to that of conventional semiconductors (1 − 10 eV).[3]

Figure 3 shows the **k**·**p** fit to the ARPES band structure with and without uniaxial strain. In the cubic phase there are three bands that are degenerate at the Γ point (dashed lines), in the absence of spin-orbit splitting. However, when an elongation of the [100] axis is applied this degeneracy is partially lifted (solid lines). While the d_{yz} band shifts up (Fig. 3(d)), the d_{xz} and d_{xy} band shift down (Fig. 3(e)). The **k**·**p** model thus accounts well for the energy shifts seen in ARPES experiments.

IV. DISCUSSION

In strained silicon, bulk degenerate valence bands are split by a compression or a dilation. The repopulation of electrons into non-degenerate bands and the suppression of inter-valley phonon scattering enhance the electron carrier mobility.[4] The enhanced mobility of the electron-doped $SrTiO_3$ films un-

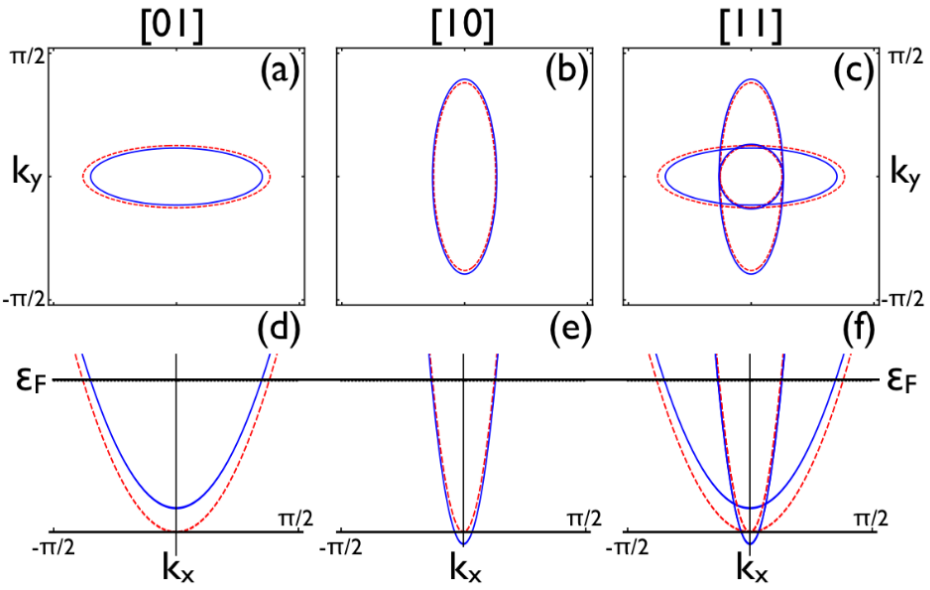

FIG. 3. (color online) Calculated band structure of the $SrTiO_3$ with (solid lines) and without strain (dashed). (a-c) Fermi surface cuts for (a) BZ [01], (b) [10], and (c) [11]. (d-e) Band structure cuts along the horizontal axes in different BZs. The energy shifts due to strain are 8.7 meV for d_{yz} band (a,d) and -4.3 meV for the d_{xz} and d_{xy} bands (b,c,e,f). A constant energy shift due to particle conservation has been ignored in this figure.

der compression can be understood in similar terms. Strain breaks the three-fold t_{2g} band degeneracy, and repopulation then reduces the average effective mass and suppresses interband scattering.[4,23,24] In particular our deformation potential difference values predict that the band shifts at the strains reported in Ref. 14 are comparable to their Fermi energies. In other words the bands should be completely altered by strains in these experiments. In this sense the large changes in mobility discovered experimentally are understandable. Since band shifts will tend to produce band depopulations and therefore higher Fermi velocities at a given total density, the sense of the mobility change is also expected. Future work that accounts for the important sources of disorder in the material might be able to account quantitatively for the mobility changes. Other more specific Fermi surface probes, for example magneto-oscillation studies under strain, would be able to confirm this interpretation. We also note that the alignment of polar domains upon uniaxial stress, which are otherwise randomly oriented and scatter charge carriers at the domain walls, can also alter the electron mobility.[7,25]

We conclude that strain-induced electronic structure changes, combined with improvements in sample quality, can further increase the efficiency and functionalities of $SrTiO_3$ and other oxide applications.[26] With the deformation potential derived in the present study, we experimentally infer the band edge lowering of 13 meV for 0.26% uniaxial strain. The t_{2g} splitting response of orbital strain is a subtle many-body effect which is difficult to estimate theoretically. The factor of 3 discrepancy between our experimental results and state of the art theory[24] provides a very specific challenge to theories of orbital order in t_{2g} perovskites. By extensively testing theoretical predictions of the deformation potentials,[24] it will be possible to provide accurate predictions of band structure changes for artificially designed strain state in heterostructure devices.

Our findings also highlight the advantage of ARPES, which is able to directly probe electronic states in momentum-space. As shown in Fig. 3(f), the three different bands overlap with a small energy splitting, which makes the detection of such small changes difficult. It is the possibility of measuring the three bands separately in different Brillouin-zones which permits the small energy shifts to be measured. Since $SrTiO_3$ represents a prototype perovskite oxide and serves as a widely used substrate for other oxides, this approach can be further extended to different types (uniaxial and biaxial) of misfit strains in oxide heterostructures utilizing *in situ* preparation of oxide films,[15,24,27,28] similar to biaxial-strained silicon formed on $Si_{1-x}Ge_x$ substrates. Given the elaborate and successful development of strain engineering in semiconductor heterojunctions, it seems clear that this is a strong motivation for further studies of strain effects in oxide systems.

In summary, we report clear change of the electronic spectral function in the electron-doped $SrTiO_3$ due to the uniaxial strain using angle-resolved photoemission spectroscopy. When the crystal is stressed, we observe the energy splitting of the Ti $3d$ t_{3g} energy bands, otherwise degenerate. Consistent with the experimental finding, we qualitatively understand the splitting using the $\mathbf{k}\cdot\mathbf{p}$ theory. Our result suggests that the mobility enhancement upon the uniaxial strain is mainly due to the degeneracy breaking along with diminished interband

scattering.

V. ACKNOWLEDGEMENT

The ALS is supported by the director of the Office of Science, Office of Basic Energy Sciences, of the U.S. Department of Energy under contract DE-AC02-05CH11231. Y. J. C., A. L. W., and K. H. acknowledge the support by the Max Planck Society. L. M. acknowledge support by a grant from the Swiss National Science Foundation (SNSF)(project PBELP2-125484). G.K. acknowledges the support of the National Science Foundation (NSF) under grant DGE-0549417 and G.K. and A.H.M. acknowledge support under NSF grant DMR-1122603.

* *e*-mail address :yjchang@uos.ac.kr

[1] D. Sekiba, K. Nakatsuji, Y. Yoshimoto, and F. Komori, Phys. Rev. Lett. **94**, 016808 (2005).

[2] G. Neuhold and K. Horn, Phys. Rev. Lett. **78**, 1327 (1997).

[3] Y. K. Sun, S. E. Thompson, and T. Nishida, Strain Effect in Semicondutors (Springer, London, 2010).

[4] M. Chu, Y. Sun, U. Aghoram, and S. E. Thompson, Annu. Rev. Mater. Res. **39**, 203 (2009).

[5] M. Abrecht, D. Ariosa, D. Cloetta, S. Mitrovic, M. Onellion, X. X. Xi, G. Margaritondo, and D. Pavuna, Phys. Rev. Lett. **91**, 057002 (2003).

[6] H. Wadati, A. Maniwa, A. Chikamatsu, I. Ohkubo, H. Kumigashira, M. Oshima, A. Fujimori, M. Lippmaa, M. Kawasaki, and H. Koinuma, Phys. Rev. Lett. **100**, 026402 (2008).

[7] D. G. Schlom, L.-Q. Chen, C.-B. Eom, K. M. Rabe, S. K. Streiffer, and J.-M. Triscone, Annu. Rev. Mater. Res. **37**, 589 (2007).

[8] T. Bak, J. Nowotony, M. Rekas, and C. C. Sorrell, Int. J. Hydrogen Energy **27**, 991 (2002).

[9] H. Ohta, S. Kim, Y. Mune, T. Mizoguchi, K. Nomura, S. Ohta, T. Nomura, Y. Nakanishi, Y. Ikuhara, M. Hirano, H. Hosono, and K. Koumoto, Nature Mater. **6**, 129 (2007).

[10] J. Mannhart and D. G. Schlom, Science **327**, 1607 (2010).

[11] N. Reyren, S. Thiel, A. D. Caviglia, L. F. Kourkoutis, G. Hammerl, C. Richter, C. W. Schneider, T. Kopp, A. S. Ruetschi, D. Jaccard, M. Gabay, D. A. Muller, J. M. Triscone, and J. Mannhart, Science **317**, 1196 (2007).

[12] Ariando, X. Wang, G. Baskaran, Z. Q. Liu, J. Huijben, J. B. Yi, A. Annadi, A. R. Barman, A. Rusydi, S. Dhar, Y. P. Feng, J. Ding, H. Hilgenkamp, and T. Venkatesan, Nature Commun. **2**, 188 (2011).

[13] M. Salluzzo, J. C. Cezar, N. B. Brookes, V. Bisogni, G. M. De Luca, C. Richter, S. Thiel, J. Mannhart, M. Huijben, A. Brinkman, G. Rijnders, and G. Ghiringhelli, Phys. Rev. Lett. **102**, 166804 (2009).

[14] B. Jalan, S. J. Allen, G. E. Beltz, P. Moetakef, and S. Stemmer, Appl. Phys. Lett. **98**, 132102 (2011).

[15] R. F. Berger, C. J. Fennie, and J. B. Neaton, Phys. Rev. Lett. **107**, 146804 (2011).

[16] C. W. Bark, D. A. Felker, Y. Wang, Y. Zhang, H. W. Jang, C. M. Folkman, J. W. Park, S. H. Baek, H. Zhou, D. D. Fong, X. Q. Pan, E. Y. Tsymbal, M. S. Rzchowski, and C. B. Eom, Proc. Natl. Acad. Sci. U.S.A. **108**, 4720 (2011).

[17] Y. J. Chang, A. Bostwick, Y. S. Kim, K. Horn, and E. Rotenberg, Phys. Rev. B **81**, 235109 (2010).

[18] R. Bistritzer, G. Khalsa, and A. H. MacDonald, Phys. Rev. B **83**, 115114 (2011).

[19] First, second-order nonlinearity of the detected angular dispersion, which appears in the angle dispersion plane (horizontal direction in Fig. 1(f)), and second, aberrations induced by changes in geometry as a function of sample polar angle relative to the photon-electron scattering plane.

[20] G. L. Bir and G. E. Pikus, Symmetry and Strain Effects in Semiconductors (Wiley, 1974).

[21] R. O. Bell and G. Rupprecht, Phys. Rev. **129**, 90 (1963).

[22] F. El-Mellouhi, E. N. Brothers, M. J. Lucero, and G. E. Scuseria, Phys. Rev. B **84**, 115112 (2011).

[23] G. Binnig, A. Baratoff, H. E. Hoenig, and J. G. Bednorz, Phys. Rev. Lett. **45**, 1352 (1980).

[24] A. Janotti, D. Steiauf, and C. G. Van de Walle, Phys. Rev. B **84**, 201304 (2011).

[25] P. Zubko, G. Catalan, A. Buckley, P. R. L. Welche, and J. F. Scott, Phys. Rev. Lett. **99**, 167601 (2007).

[26] J. Son, P. Moetakef, B. Jalan, O. Bierwagen, N. J. Wright, R. Engel-Herbert, and S. Stemmer, Nature Mater. **9**, 482 (2010).

[27] Y. J. Chang, C. H. Kim, S. H. Phark, Y. S. Kim, J. Yu, and T. W. Noh, Phys. Rev. Lett. **103**, 057201 (2009).

[28] A. Tebano, A. Orsini, P. G. Medaglia, D. Di Castro, G. Balestrino, B. Freelon, A. Bostwick, Y. J. Chang, G. Gaines, E. Rotenberg, and N. L. Saini, Phys. Rev. B **82**, 214407 (2010).